Check for updates

OPEN

Hydrogen–nitrogen plasma assisted synthesis of titanium dioxide with enhanced performance as anode for sodium ion batteries

Hongmei Wang[1], Jie Xiong[1], Xing Cheng[2], Ge Chen[2✉], Thomas Kups[1], Dong Wang[1✉] & Peter Schaaf[1]

Sodium ion batteries are considered as one of the most promising energy storage devices as lithium ion batteries due to the natural abundance of sodium. TiO_2 is very popular as anode materials for both lithium and sodium ion batteries because of the nontoxicity, safety and great stabilities. However, the low electronic conductivities and inferior sodium ion diffusion make it becoming a great challenge to develop advanced TiO_2 anodes. Doping heteroatoms and incorporation of defects are believed to be great ways to improve the electrochemical performance of TiO_2 anodes. In this work, commercial TiO_2 (P25) nanoparticles was modified by hydrogen and nitrogen high-power plasma resulting in a disordered surface layer formation and nitrogen doping as well. The electrochemical performances of the samples as anode materials for sodium ion batteries was measured and the results indicated that after the hydrogen–nitrogen plasma treatment, H–N-TiO_2 electrode shows a 43.5% of capacity higher than the P-TiO_2 after 400 cycles long-term discharge/charge process, and the samples show a good long cycling stability as well, the Coulombic efficiencies of all samples are nearly 99% after 50 cycles which could be sustained to the end of long cycling. In addition, hydrogen–nitrogen plasma treated TiO_2 electrode reached the stable high Coulombic efficiency earlier than the pristine material. High resolution TEM images and XPS results indicate that there is a disordered surface layer formed after the plasma treatment, by which defects (oxygen vacancies) and N-doping are also introduced into the crystalline structure. All these contribute to the enhancement of the electrochemical performance.

Rechargeable sodium ion batteries (SIBs) have been considered as the competitive alternative to lithium ion batteries because of some special merits, such as environment friendly, low cost and especially abundant alkali element widely distributed on earth[1–3]. However, there is a big challenge that the ion radius of Na ions are ~ 70% larger than that of Li ions, so finding proper electrode materials which could provide big interstitial space to accommodate sodium ions and allow reversible and rapid ion insertion/extraction[3] is a challenging topic at the moment. Recently, many efforts have been made to explore advanced anode materials for sodium ion batteries. Firstly, carbonaceous material is an important choice which is very cheap however carbonaceous materials show undesired properties with low capacities and/or poor cycle performance[4]. Secondly, Ti-based materials is a promising anode materials for sodium ion batteries, including $Na_2Ti_3O_7$, $Na_{0.66}[Li_{0.22}Ti_{0.78}]O_2$, $Li_4Ti_5O_{12}$, and titanium dioxide (TiO_2)[5]. Moreover, other materials based on alloying reactions (such as Sn, Sb, P and their compounds e.g. inter-metallics, oxides, sulfides, and phosphides)[6–10] and conversion reactions (oxides and sulfides, e.g. Fe_2O_3,

[1]Fachgebiet Werkstoffe der Elektrotechnik, Institut für Werkstofftechnik und Institut für Mikro-Und Nanotechnologien MacroNano®, TU Ilmenau, Gustav-Kirchhoff-Str. 5, 98693 Ilmenau, Germany. [2]Beijing Key Laboratory for Green Catalysis and Separation, College of Environmental and Energy Engineering, Beijing University of Technology, 100124 Beijing, People's Republic of China. ✉email: chenge@bjut.edu.cn; dong.wang@tu-ilmenau.de

Fe_3O_4, FeOOH, MoO_3, CuO, Mn_3O_4, $NiCo_2O_4$ and MoS_2)[11, 12] attract some attentions as well. In addition, organic compounds are also potential anode materials for sodium ion batteries[13–15].

Titanium dioxide (TiO_2) with various polymorphs like anatase[16], rutile[17], amorphous[18] TiO_2 and TiO_2-B[19] as anode materials have been investigated, and it is generally considered as a promising energy storage material because of the low cost, environmental friendliness, intrinsic safety, abundant resources, high power density and long cycle life[20, 21]. Nevertheless, the big limitation of using TiO_2 as anode for sodium ion batteries is its inherent low electrical conductivity. In order to solve this problem, firstly, surface coating could be a good method to improve the TiO_2 conductivity, especially introducing carbon additives to enhance the electrical conductivity of TiO_2 anodes, like amorphous carbon, CNTs and graphene have been widely studied as conductive agents[22–27]. Secondly, designing nanosized TiO_2, for example nanotubes[28], nanoparticles[29], nanorods[28] and nanofiber[30], petal-like TiO_2[20], is also a good way because the nanosized structure could effectively enlarge the active area of the material and shorten the ion diffusion path during electrochemical processes. He et al.[31] reported a hierarchical rod-in-tube TiO_2 with a uniform carbon coating as the anode material for sodium-ion batteries by a facile sol-vothermal method. The author claimed that this unique structure consists of a tunable nanorod core, interstitial hollow spaces, and a functional nanotube shell assembled from two-dimensional nanosheets. What's more, het-eroatom doping like N, S, B, P or Nb[32–39], which could substantially increase the electronic conductivity and the specific capacities for the sodium storage. A nitrogen-doped carbon layer coated yolk-like TiO_2 electrode could offer a superior high capacity of 115.9 mAh/g[1] at 20 C (6700 mA/g)[27]. It is clear that the key factor to improve the electrochemical performance of TiO_2 is to combine strategies of shortening sodium-ion diffusion distance and improving electronic conductivity. In addition, the produced oxygen vacancies or trivalent titanium spe-cies can be formed to improve the electrical conductivity as well[3, 32, 40]. Wang and co-workers proposed a novel and facile N_2 plasma assisted annealing strategy, by which nitrogen heteroatoms and rich oxygen vacancies are incorporated into the TiO_2 crystal simultaneously, leading to highly enhanced electronic conductivity[40]. In addi-tion, previous work of our group has already shown that plasma treatment is a promising method to enhance the performance of TiO_2 as anode material. A hydrogen plasma treated TiO_2 as anode for lithium ion batteries shows that the treated black TiO_2 shows great improvement for fast lithium storage[41]. Furthermore, another work shows that nitrogen plasma treated TiO_2 with a disordered surface layer and nitrogen doping shows an enhanced performance for sodium ion batteries[32].

Here, we developed a combination of hydrogen and nitrogen plasma assisted strategy to synthesize nitrogen doping and defect-rich (oxygen vacancies) TiO_2 electrode that demonstrated an enhanced performance as anode material of sodium ion batteries. In our research, there are three electrodes which are tested, pristine commer-cial TiO_2 as control sample (named as P-TiO_2), high-power hydrogen plasma treated TiO_2 (named as H-TiO_2) and high-power nitrogen plasma treated H-TiO_2 (named as H–N-TiO_2). When used as anode materials, the H–N-TiO_2 shows the best sodium storage performance, and both H-N-TiO_2 and H-TiO_2 demonstrated much higher specific capacities than pristine TiO_2, and also the long-term performance results are promising. The high-resolution images of transmission electron microscopy shown that there is a disordered surface layer was formed after the plasma treated materials, no matter the hydrogen or nitrogen plasma process. For this improve-ment of the electrodes, we could attribute it to the disordered surface layer, the oxygen vacancies and the nitrogen doping, and all of them play significant roles in enhancing the electrochemical sodium storage performance.

Experimental section

Sample preparation.
The sample preparation process is similar with our previous work[32, 42]. Commercial TiO_2 (P25) nanoparticles were purchased from Sigma-Adlrich and used without further purification. 0.15 g TiO_2 nanoparticles were dispersed in 30 ml ethanol with ultrasonic support and drop-casted onto a 6-inch Si wafer. The drop-casting process was repeated several times to achieve TiO_2 mass loading of about 0.8 mg cm^{-2} (sample mass loading should be no more than 1.5 mg cm^{-2} to avoid inhomogeneous plasma treatment). Before each drop, the previous dropped ethanol must be volatilized totally so that a homogenous distribution of the nanoparticles on the silicon wafer can be obtained.

The drop-casted wafer was transferred into a chamber for the plasma treatment, and the instrument of induc-tively coupled plasma enhanced chemical vapor deposition (ICP-CVD, Plasmalab 100, Oxford) was used. Before the plasma treatment process, a preconditioning process takes place at 300 °C to ensure the quality of plasma treatment. Then H_2 plasma treatment was performed at 300 °C for 30 min, the ICP power was 3000 W, chamber pressure was 3.52–3.76 Pa, and H_2 flow rate was 50 sccm. Afterwards, N_2 plasma treatment was performed at 300 °C for 30 min, the ICP power was 3000 W, the chamber pressure was 3.52–3.76 Pa, and N_2 flow rate was 30 sccm. After all plasma treatment, H-TiO_2 and H–N-TiO_2 nanoparticles were obtained and scratched from the Si wafer for further investigations and application measurements.

Characterization.
The crystal structure of the TiO_2 nanoparticles was characterized by X-ray diffraction (XRD, SIEMENS D5000) with Cu Kα radiation. The sample was scanned from $2\theta = 10°–80°$ at a rate of 0.03° s^{-1} in Bragg–Brentano geometry. Then, transmission electron microscopy (TEM, Tecnai F20) was used to charac-terize the nanoparticle morphology and microstructure. Ultraviolet–visible (UV–Vis) absorption spectra were measured by using a Cary 5000 UV–Vis-NIR. Finally, the samples were analyzed by XPS using a spectrometer (PHI Quantera SXM) with monochromatized Al-Kα radiation.

Electrochemical experiments.
The electrochemical performances of the materials used as anode for sodium-ion batteries were tested via 2032 coin half-cells, which were assembled in an argon-filled glove box, where both the moisture and oxygen contents were less than 0.5 ppm. The working electrode was immersed in a mixture, which consist of active material, super carbon black and polyvinylidene in ratio of 70: 15: 15, toward
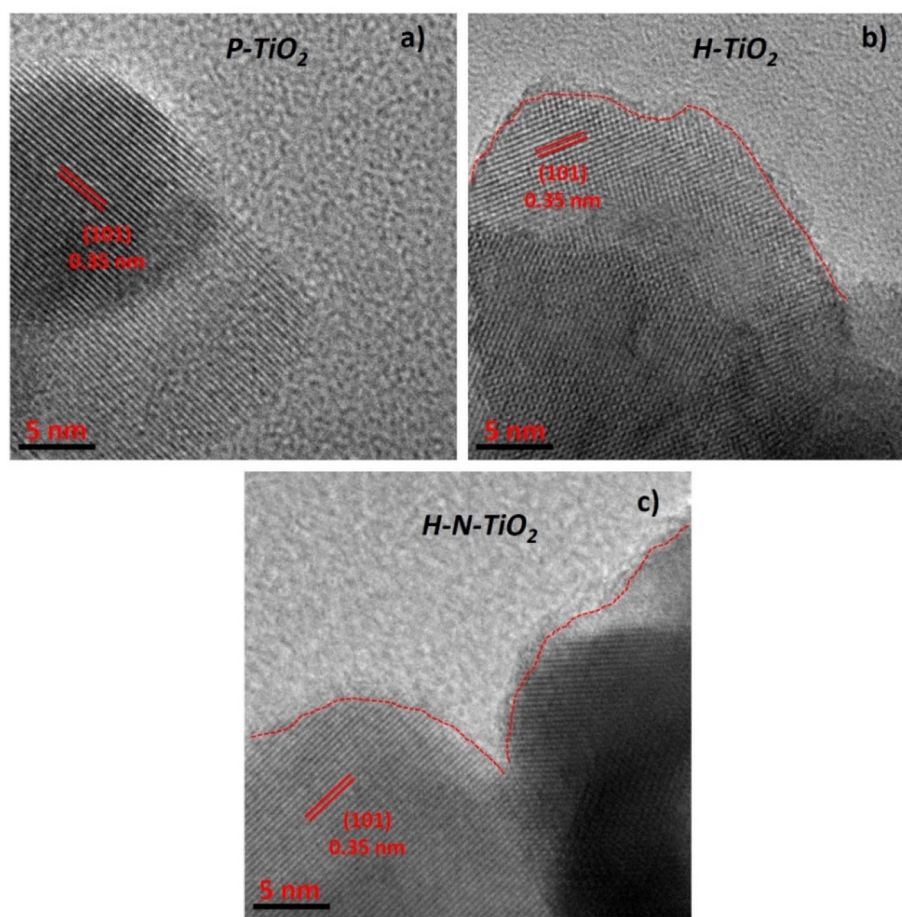
Figure 1. High resolution TEM images of (**a**) the pristine (P-TiO$_2$) nanoparticles, (**b**) the nanoparticles treated with H$_2$ plasma (H-TiO$_2$), and (c) the nanoparticles treated with both H$_2$ and N$_2$ plasma (H–N-TiO$_2$).

forming a homogeneous slurry in N-methyl-pyrrolidone (NMP). Then, the slurry was pasted onto stainless steel foil with a sample loading of about 1.8 mg cm^{-2}. The handled electrode was dried for 12 h at 120 °C under vacuum. Glass fiber (GF/D, Whatman) and pure sodium foil (Aldrich) were respectively used as a separator and the counter electrode. The electrolyte was 1 M NaPF$_6$ in a mixture of ethylene carbonate and diethyl carbonate, in a ratio of 50:50. For the galvanostatic measurement, a battery tester (Neware, Shenzhen, China) was used. Cyclic voltammetry (CV) was applied in a potential range from 3.0 to 0.01 V at a scan rate of 0.5 mV s^{-1} by a potentiostat (VMP3, BioLogics, France). Furthermore, the alternating current (AC) impedance of the samples were determined by a same potentiostat and the impedance spectra, which were acquired via a sine wave with an amplitude of 5.0 mV in a frequency range from 100 kHz to 0.01 Hz after discharging/charging for 5 cycles at a current density of 1 A g^{-1}.

Results and discussion

Figure 1 shows the high-resolution TEM images of the pristine TiO$_2$ nanoparticles and the TiO$_2$ nanoparticles after plasma treatments. We could see that all TiO$_2$ nanoparticles were highly crystallized, and the interplane spacing of ordered lattices is measured to be closed to 0.35 nm, which could be attributed to (101) planes of the anatase crystal phase. Moreover, we could find that the crystal lines of plasma treated material (H-TiO$_2$ and H–N-TiO$_2$) do not arrange clearly compared with the pristine TiO$_2$, and there are some crossovers of the fringes which may be a partially dislocation or defects in the TiO$_2$. What's more, a disordered layer was found in Fig. 1b, c, and the thickness of the disordered surface layer is about 1.5 nm, we think this is due to the high-power plasma treatment processes. According to previous report[43], the thickness of the disordered surface layer could be increase upon the plasma treatment time, after 20 min treatment, the thickness reaches to around 1.5–2.2 nm and the Electron paramagnetic resonance (EPR) result indicated that hydrogen plasma treatment is very effective to produce Ti^{3+} species and oxygen vacancies, which resulted in the disordered surface layer formation.

The XRD patterns of the samples are shown in Fig. 2a, from which we could see there are two different phases of TiO$_2$, anatase and rutile. The peaks appearing at 2θ = 25.4°, 36.0°, 37.8°, 38.5°, 48.0°, 55.0°, 62.7°, 70.2°, 75.1° and 76.0° correspond to the (101), (103), (004), (112), (200), (211), (204), (220), (215) and (301) diffractions of anatase TiO$_2$ (PDF No. 21-1272), respectively. And the other peaks which located at 2θ = 27.3°, 36.0°, 41.2°, 42.5°, 54.0°, 56.6° and 68.8° could be attributed to the (110), (101), (111), (210), (105), (220) and (301) diffractions of

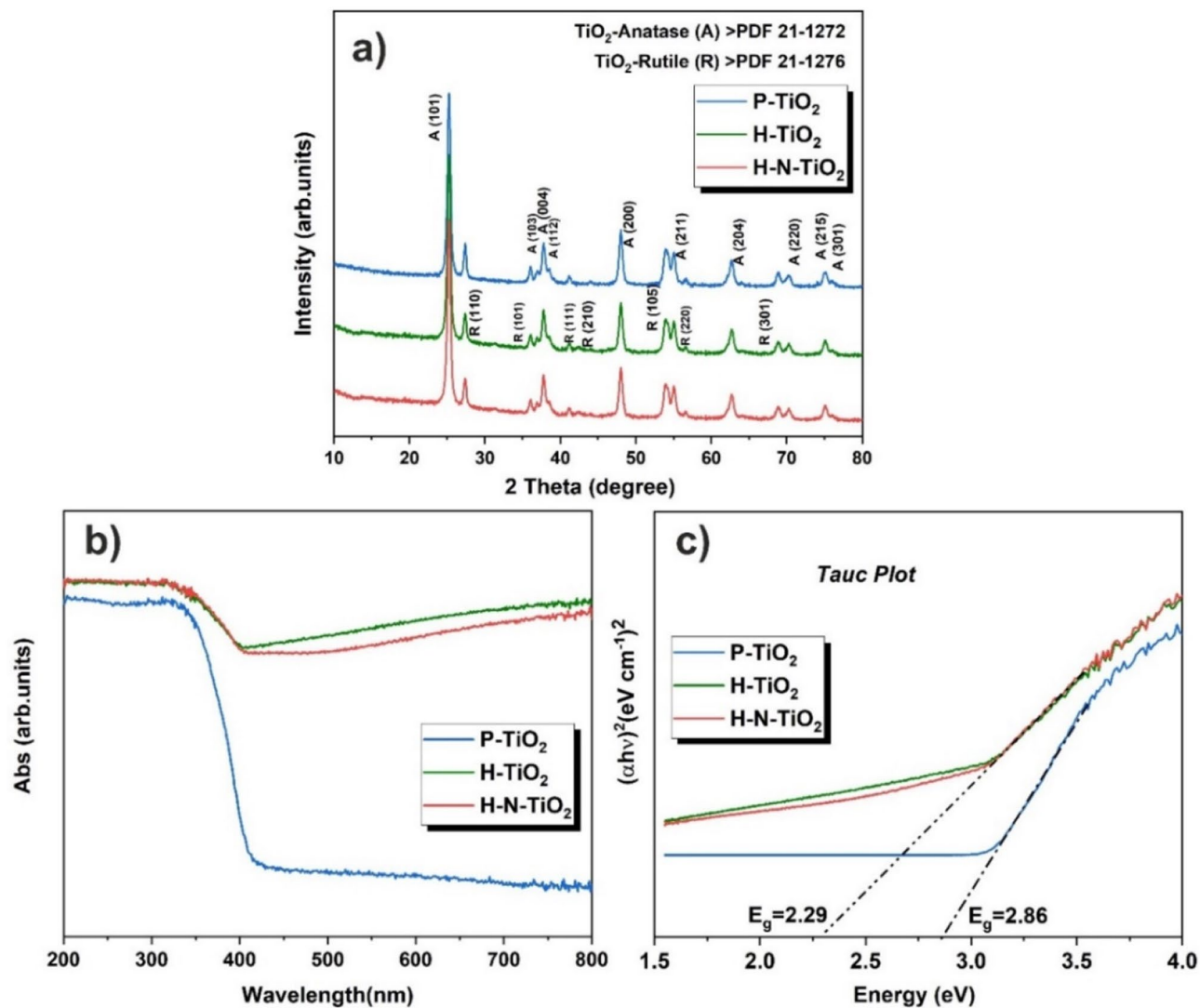**Figure 2.** (**a**) X-ray diffraction patterns of P-TiO$_2$, H-TiO$_2$ and H–N-TiO$_2$; (**b**) UV–Vis absorption spectra of P-TiO$_2$, H-TiO$_2$ and H–N-TiO$_2$ and (**c**) Tauc plots to obtain the band gap.

rutile TiO$_2$ (PDF No. 21-1276), respectively. The intensities of the peaks in the P-TiO$_2$ are slightly higher than those in the plasma treated materials. Except these small differences, all the diffraction peaks are almost the same. In addition, the peaks of nitrides were not clearly observed in the patterns, probably due to the low amount of doping contents and also the homogeneous distribution of N in the sample[44, 45]. The UV–Vis absorbance of the samples was investigated and Tauc plots were calculated to determine the band gap energy of the materials. As shown in Fig. 2b, P-TiO$_2$ shows the absorption edge at around 427 nm, while after plasma treatment, the absorption edge shifted to ~ 685 nm for both H-TiO$_2$ and H–N-TiO$_2$. The strongly enhanced absorption of the plasma treated materials in the region of visible light indicates that the high-power plasma treatment can result in a reduction effect and oxygen vacancies are formed on the materials surface[41, 43]. Tauc plots (Fig. 2c) clarifies the decline of band gap energy of the materials from 2.86 to 2.29 eV due to the hydrogenation process[41] and nitrogen doping[46–48].

XPS was used to investigate the surface chemical structure details of the obtained samples (shown in Fig. 3), Ti, O and C elements could be observed from the survey spectra in Fig. 3a. For the further analysis of the chemical structure of the investigated TiO$_2$ samples, high-resolution XPS spectra of all elements are processed. Figure 3b shows the high-resolution spectra of Ti 2p, from the spectra we could see there are two typical peaks which centered at 464.3 and 458.5 eV for all samples. They could be attributed to the Ti 2p$_{1/2}$ and Ti 2p$_{3/2}$, respectively, which represent the characteristic peaks of Ti^{4+}. What's more, compared to the other two samples, the Ti 2p$_{3/2}$ peak of H-TiO$_2$ shifted to the lower binding energy slightly, but the peak difference is so weak and we would say that the change of chemical environment of titanium is not obvious after high-power plasma treatment.

Figure 3c shows the XPS spectra of O 1s, there is one main peak located at 529.7 eV for the pristine and hydrogen treated materials, which is attributed to bulk oxygen O^{2-}. For H–N-TiO$_2$, two new characteristic peaks appear after plasma treatment, which are centered at 530.2 and 531.9 eV, corresponding to the chemisorbed oxygen of the surface hydroxyl, absorbed H$_2$O, absorbed O$_2$ or the surface contamination[49]. Further, the peak centered at
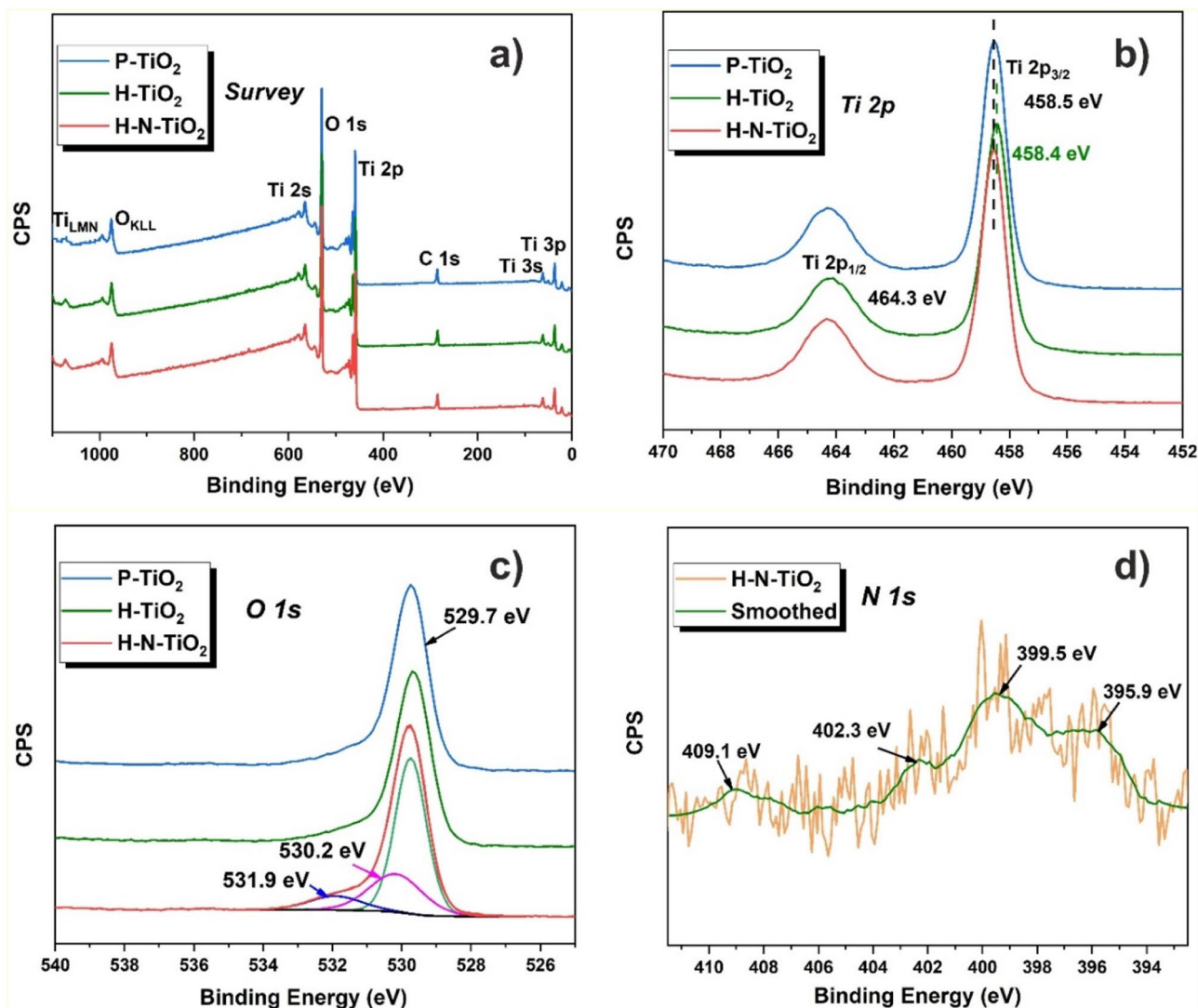
Figure 3. (**a**) XPS survey spectra of TiO_2 electrodes; (**b**) Ti 2p spectra of TiO_2 electrodes; (**c**) O 1s spectra of TiO_2 electrodes; (**d**) N 1s spectrum of H–N-TiO_2.

531.9 eV is attributed to the presence of Ti–O–N bonds[49, 50], which indicates the formation of Ti–O–N bonds after the hydrogen and nitrogen plasma treatment.

In addition, the high-resolution XPS spectrum of N 1s of H–N-TiO_2 is displayed in Fig. 3d. In accordance with a previous report[32], the 30-min nitrogen plasma treatment can result in about 0.5 at% of nitrogen doping in the material. There are four characteristic peaks, which are located at 395.9, 399.5, 402.3 and 409.1 eV, respectively. Firstly, according to some reports[51, 52] the peak of N 1s located at 395.9 eV can be attributed to O–Ti–N linkages, which comes from the doping of N atoms into the TiO_2 lattice. Another peak at 399.4 eV can be attributed to interstitial N[49]. Furthermore, two other peaks at 402.3 and 409.8 eV belong to NO or NO_2 type species which usually appear at binding energies higher than 400 eV[50]. From the above observations, the chemical states of the nitrogen doped TiO_2 exist with the form of N–Ti–O and Ti–O–N[46]. Many research works have been reported that the role of N species on the electrical conductivity of TiO_2 is mainly related to the decrement of the band gap, because nitrogen doping can elevate the valence band maximum[53].

Electrochemical performances of sodium ion batteries

The electrochemical performances of the TiO_2 employed as anode materials for sodium-ion batteries were evaluated in coin half-cells using sodium metal as the counter electrode. Firstly, the cycle voltammetry (CV) plots which were evaluated at a scan rate of 0.5 mV/s at a voltage range of 0.01–3.0 V for 3 cycles of each sample are shown in Fig. 4. All of the TiO_2 electrodes display the typical CV curves of TiO_2 anode for SIBs[29, 54]. From the first cycle, irreversible broad cathode peaks at wide potential range of 0.01–0.5 V are observed for all samples (Fig. 4), which can be attributed to the irreversible sites for Na-ion insertion in the crystal lattice defects, electrolyte and other organic material decomposition and the solid electrolyte interface (SEI) layer formation[54, 55]. From the second and third cycles, there are only the peaks at around 0.78 and 0.85 V are shown in the CV profiles for all obtained samples (Fig. 4), which are corresponding to the reversible insertion/de-insertion of Na into/from the
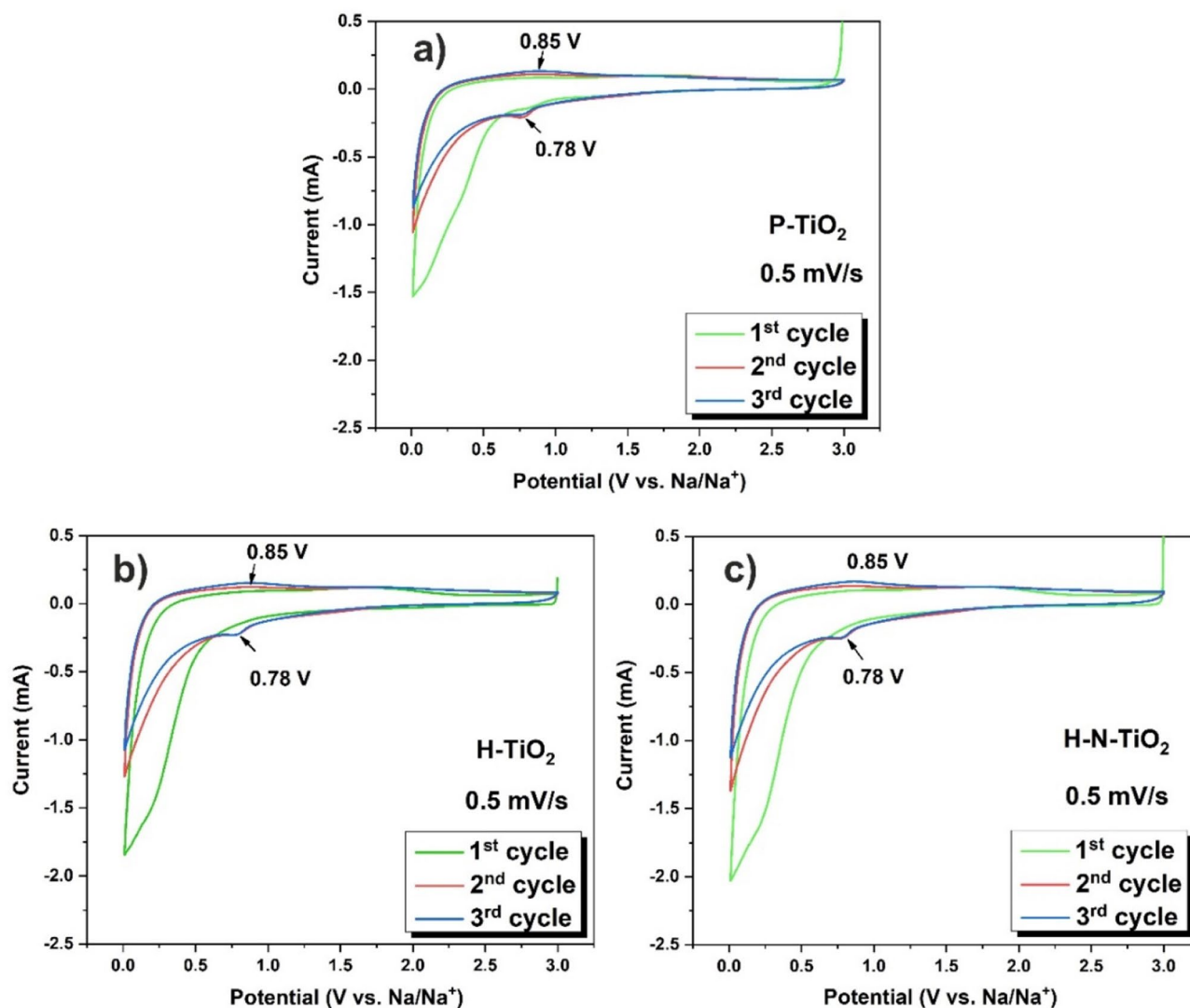
5

Figure 4. (**a**) CV curves of TiO$_2$ electrodes measured at a scan rate of 0.5 mV s^{-1} for 3 cycles, (**a**) P-TiO$_2$; (**b**) H-TiO$_2$; (**c**) H–N-TiO$_2$.

electrodes. Moreover, except the first cycle, the CV curves of all three samples overlapped well for the second and third cycles, which demonstrated good cycling stability and the high reversibility of TiO$_2$ electrodes. What's more, the peak current of the H-TiO$_2$ and H–N-TiO$_2$ are wider and stronger than those of the P-TiO$_2$ electrode, and it means the plasma treated materials show better sodium storage performances (Fig. 4b,c).

The rate performances of all samples are given in Fig. 5a, b, all obtained samples were measured at current densities of 0.1, 0.5, 1, 2 and 5 C for 4 cycles of every step, and then the current densities came back to 0.1 C for 10 cycles (1C = 335 mA/g). The first cycle discharge/ charge specific capacities of P-TiO$_2$, H-TiO$_2$ and H–N-TiO$_2$ electrodes, are 584.28/112.08, 562.86/117.70 and 603.60/121.65 mAh/g, respectively. A very low coulombic efficiency for about 20% are obtained for all the materials at the first cycles. The irreversible capacities of the electrodes were mainly caused by the occurrence of the side reactions which could form a solid-electrolyte interface (SEI) layer. It is hard to say which treated material shown a better electrochemical performance, but we are sure that the plasma treatment methods have a good effect on the TiO$_2$ anode materials for SIBs. In order to further understand the improved higher performance of the TiO$_2$ electrodes, electrochemical impedance spectra (EIS) was evaluated in the frequency range of 100 kHz to 0.01 Hz (as shown in Fig. 5c). The spectra were fitted by Zview software using an equivalent circuit mode. Here, R$_s$ is the internal resistance in the batteries and R$_1$ is charge transfer resistance on the interface of electrode and electrolyte. CPE represent a constant phase element and the sloping line in the low-frequency region related to W1, which is called Warburg impendence, could be attributed to the diffusion resistance in the electrode[56]. The charge transfer resistance of the P-TiO$_2$ is about 137 Ω according to the fitted result, and increased a bit for the H-TiO$_2$ electrode. While the charge transfer resistance of H–N-TiO$_2$ (ca. 66 Ω) is about half of the P-TiO$_2$, which means that the nitrogen doping is an easy and effective way to improve the electrical conductivity and the charge transfer reactions of the TiO$_2$ anode material for sodium ion batteries. From our previous work, an individual nitrogen plasma treated TiO$_2$ shown the similar result[32].

The long cycling stabilities of the materials were evaluated at a current rate of 1 C for 400 cycles. As is shown in Fig. 6a,c, the first discharge/charge specific capacities of P-TiO$_2$, H-TiO$_2$ and H–N-TiO$_2$ electrode are
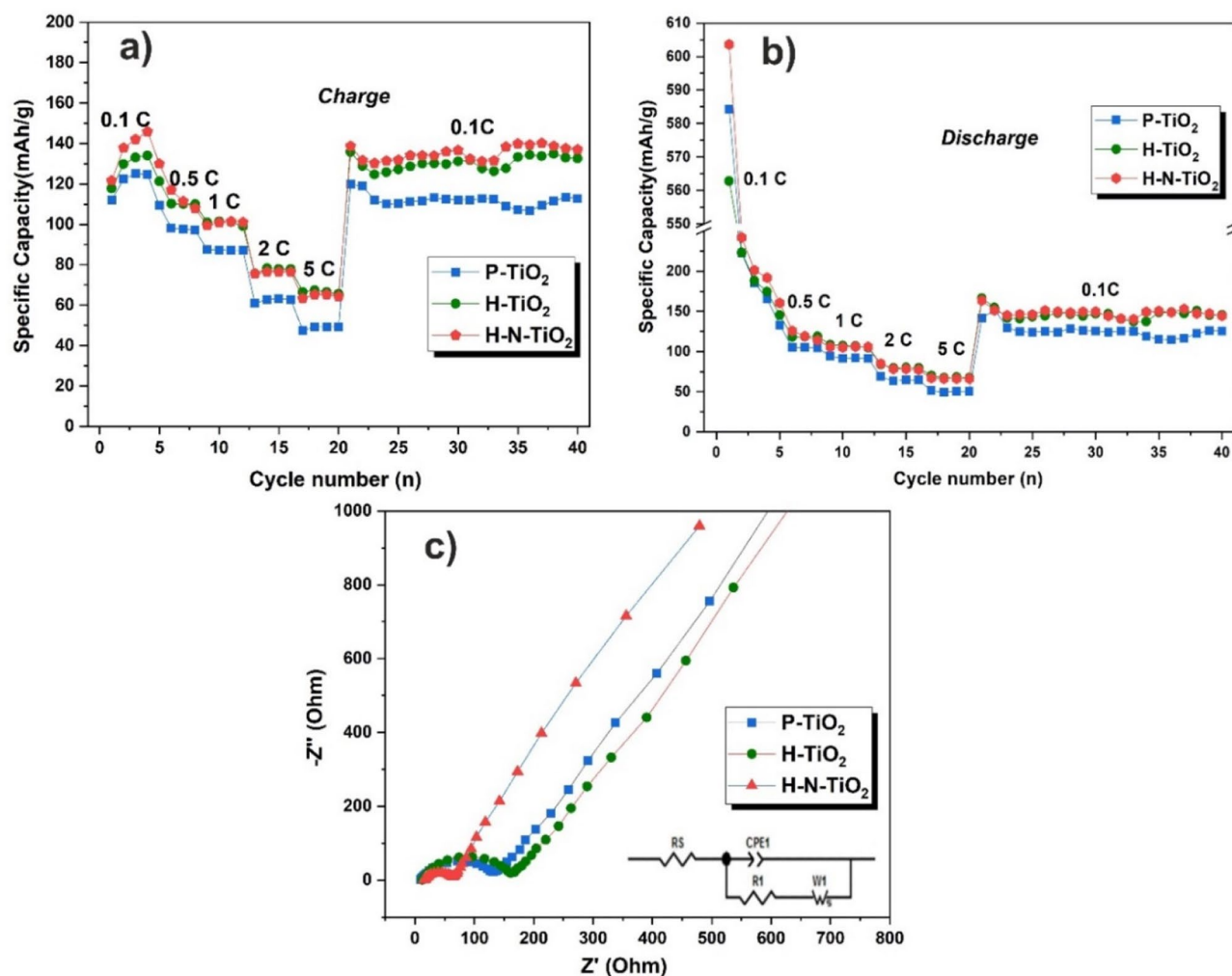
Figure 5. Rate performances of TiO_2 electrodes at the current densities of 0.1, 0.5, 1.0, 2.0 and 5.0 C, (**a**) charge, (**b**) discharge; (**c**) Nyquist plots of TiO_2 electrodes.

304.73/64.23, 325.76/69.37 and 338.07/72.54 mAh/g, respectively. It is very similar to the rate performance, all of the materials show a very low Coulombic efficiency in the first cycle, about 21%. The low Coulombic efficiency of all samples is due to the large ion radius of sodium and low theoretical capacity of TiO_2 anodes, which can result in high irreversible capacities of anodes for sodium ion batteries. Secondly, the TiO_2 materials we used in this work is just normal nanoparticles, we don't have special structure to provide large amounts of active sites for the electrochemical reactions. In addition, the nitrogen concentration after plasma treatment is also very low compared with some previous reported works[37, 57], but we could still see the big improvement of the materials as anode with the effect of plasma treatment. After about 20 cycles, the materials which were treated with hydrogen and nitrogen plasma, show higher capacities than the pristine TiO_2. Especially for the H–N-TiO_2, the discharge/charge capacities for the 400th cycles are 68.05/66.85 mAh/g, while the P-TiO_2 just show specific capacities of 47.40/46.44 mAh/g, it means that H–N-TiO_2 showing a 43.5% of capacity higher than the P-TiO_2 after 400 long-term cycles.

Compared with our previous work[32], hydrogen and nitrogen double plasma treatment give an improvement on the specific capacities (increased around 10% at 400th cycle) than an individual nitrogen plasma treatment, it means the hydrogenation process also makes contributions on enhancing the sodium storage performances. All of the samples show a good long cycling stability, the Coulombic efficiencies of them are nearly 99% after 50 cycles, and this could be sustained to the end of long cycling (Fig. 6e). In addition, there are some fluctuations of the capacity upon the further cycling for all samples. The reason is not clear. However, Wu[58] and co-workers reported that during the reaction of the large size of sodium ions with the electrodes, more electrolyte penetrates from the surface of electrode into the bulk and then more active materials are participated into the reaction with the increasing of the cycling numbers; also, some other reported works[59, 60] claim that the deposition of transition metal compounds on the anode electrode would induce the chemical degradation of SEI film. When the accumulation of produced metallic titanium reached to a certain amount, metallic titanium may catalyze and accelerate the decomposition of SEI film with the electrolyte, which could cause a sudden rise of specific capacity of electrodes.
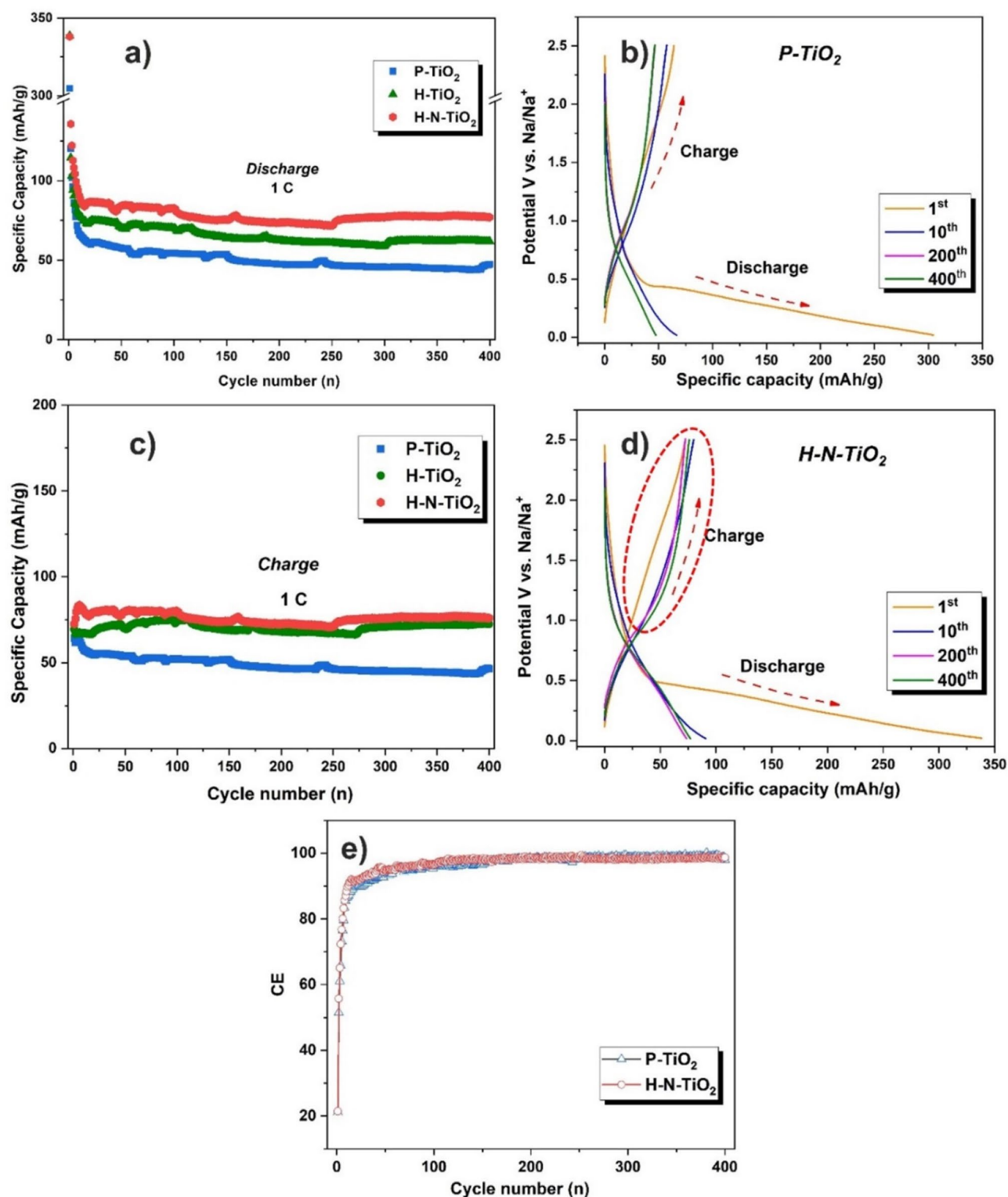
Figure 6. Long term cycling performances of electrodes at a current rate of 1 C (**a**) discharge; (**c**) charge; Galvanostatic discharge/charge curves of electrodes at different cycles (**b**) P-TiO$_2$; (**d**) H–N-TiO$_2$; (**e**) Coulombic efficiencies for long cycling performances of P-TiO$_2$ and H–N-TiO$_2$.

Because the different performances of the P-TiO$_2$ and H–N-TiO$_2$ during the long-term cycling process, so we want to get some more details from the long-term performance galvanostatic discharge and charge curves, as shown in Fig. 6b,d. The first cycle of these two materials are very similar for the charge and discharge process.
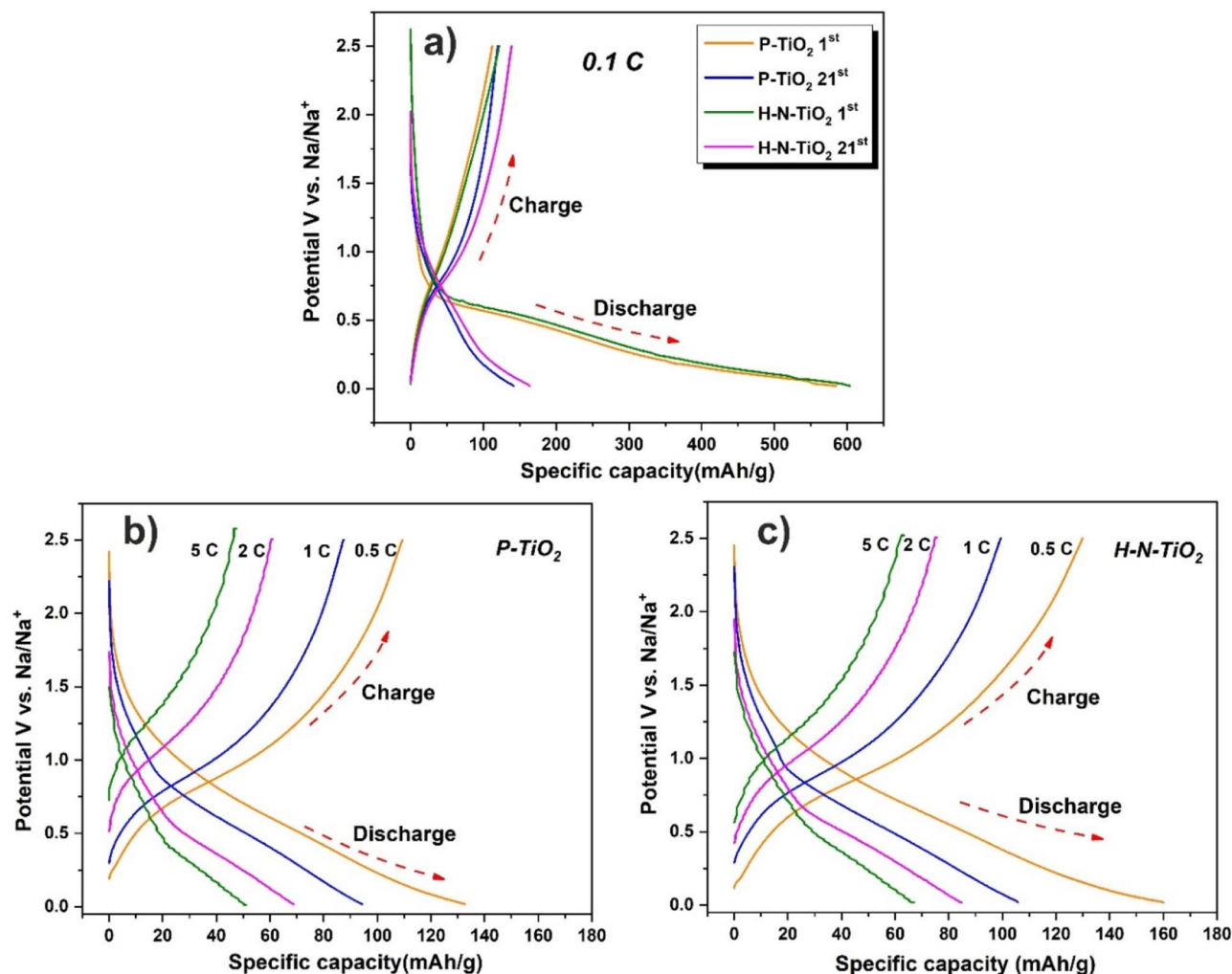
Figure 7. (**a**) Galvanostatic discharge/charge curves of P-TiO$_2$ and H–N-TiO$_2$ electrodes at current density of 0.1 C. Galvanostatic discharge/charge curves at different current densities (**b**) P-TiO$_2$, (**c**) H–N-TiO$_2$.

But after several cycles, we could see that something is different for the charge curves. The H–N-TiO$_2$ shown a slow potential increase from ~ 1.0 to 2.0 V (as shown by the red circle in Fig. 6d), it may cause by the amorphous surface layer which is good for the sodium ions transport in the material and also the nitrogen doping could greatly increase the conductivity of the TiO$_2$ materials. Figure 7a is the 1st and 21st galvanostatic discharge/charge curve of P-TiO$_2$ and H–N-TiO$_2$ electrodes at the current density of 0.1 C. The 1st discharge curve of H–N-TiO$_2$ indicate a longer voltage plateau from 0.5 to 0.01 V compared to P-TiO$_2$, which is matched well with the CV results and also tell us that H–N-TiO$_2$ possesses a higher sodium ion storage ability. The 21st cycle galvanostatic discharge/charge curves show the similar result. According to the results mentioned above, firstly, the achieved discharge specific capacity of H–N-TiO$_2$ is higher than the P-TiO$_2$ electrode; secondly, for H–N-TiO$_2$, the higher charge capacities could be obtained when the charge voltage is higher than 1.0 V, means that the reversible charge capacities of H–N-TiO$_2$ are higher than the P-TiO$_2$. In addition, Fig. 7b, c) show the galvanostatic discharge/charge curves of the electrodes at different current densities. The discharge/charge capacities of H–N-TiO$_2$ are all higher than that of P-TiO$_2$. And much slower performance fading of H–N-TiO$_2$ is obtained at all different current stages. All these results give solid proofs of the considerable performance improvement of the H–N-TiO$_2$ electrode.

Conclusions

In summary, we developed a combination of hydrogen and nitrogen plasma assisted strategy to synthesize nitrogen doping and defect-rich TiO$_2$ electrode that demonstrated an enhanced performance as anode material of sodium ion batteries. When used as anode materials, the H–N-TiO$_2$ shown the best sodium storage performance, and then is H-TiO$_2$, both of them demonstrated much higher specific capacities than pristine TiO$_2$. The rate performances of H-TiO$_2$ and H–N-TiO$_2$ are significantly improved compared to P-TiO$_2$. What's more, H–N-TiO$_2$ shows a 43.5% of capacity higher than the P-TiO$_2$ after 400 cycles long-term discharge/charge process, and the samples show a good long cycling stability as well, the Coulombic efficiencies of all samples are nearly 99% after 50 cycles, and this could be sustained to the end of long cycling. In addition, H–N-TiO$_2$ reached the stable high Coulombic efficiency earlier than the pristine material. The high-resolution images of transmission

electrons microscopy shown that there is a disordered surface layer was formed after the plasma treated materials, no matter the hydrogen or nitrogen plasma process. For this improvement of the electrodes, the disordered surface layer, the oxygen vacancies and the nitrogen doping play significant roles together in enhancing the electrochemical sodium storage performance.

References

1. Li, G., Blake, G. R. & Palstra, T. T. M. Vacancies in functional materials for clean energy storage and harvesting: the perfect imperfection. *Chem. Soc. Rev.* **46**, 1693–1706 (2017).
2. Zhao, C. *et al.* Ultrahigh rate and long-life sodium-ion batteries enabled by engineered surface and near-surface reactions. *Adv. Mater.* **30**, 1–9 (2018).
3. Gan, Q. *et al.* Defect-assisted selective surface phosphorus doping to enhance rate capability of titanium dioxide for sodium ion batteries. *ACS Nano* **13**, 9247–9258 (2019).
4. Pan, H., Hu, Y. S. & Chen, L. Room-temperature stationary sodium-ion batteries for large-scale electric energy storage. *Energy Environ. Sci.* **6**, 2338–2360 (2013).
5. Yu, L. *et al.* Understanding fundamentals and reaction mechanisms of electrode materials for Na-ion batteries. *Small* **14**, 1–22 (2018).
6. Mortazavi, M., Deng, J., Shenoy, V. B. & Medhekar, N. V. Elastic softening of alloy negative electrodes for Na-ion batteries. *J. Power Sources* **225**, 207–214 (2013).
7. Wu, L. *et al.* SiC-Sb-C nanocomposites as high-capacity and cycling-stable anode for sodium-ion batteries. *Electrochim. Acta* **87**, 41–45 (2013).
8. Wu, L. *et al.* Sb-C nanofibers with long cycle life as an anode material for high-performance sodium-ion batteries. *Energy Environ. Sci.* **7**, 323–328 (2014).
9. Xiao, L. *et al.* High capacity, reversible alloying reactions in SnSb/C nanocomposites for Na-ion battery applications. *Chem. Commun.* **48**, 3321–3323 (2012).
10. Wu, L. *et al.* A tin(ii) sulfide-carbon anode material based on combined conversion and alloying reactions for sodium-ion batteries. *J. Mater. Chem. A* **2**, 16424–16428 (2014).
11. Klein, F., Jache, B., Bhide, A. & Adelhelm, P. Conversion reactions for sodium-ion batteries. *Phys. Chem. Chem. Phys.* **15**, 15876–15887 (2013).
12. Bommier, C. & Ji, X. Recent development on anodes for Na-ion batteries. *Isr. J. Chem.* **55**, 486–507 (2015).
13. Choi, A. *et al.* 4,4′-Biphenyldicarboxylate sodium coordination compounds as anodes for Na-ion batteries. *J. Mater. Chem. A* **2**, 14986–14993 (2014).
14. Chen, L., Li, W., Wang, Y., Wang, C. & Xia, Y. Polyimide as anode electrode material for rechargeable sodium batteries. *RSC Adv.* **4**, 25369–25373 (2014).
15. Weeraratne, K. S., Alzharani, A. A. & El-Kaderi, H. M. Redox-active porous organic polymers as novel electrode materials for green rechargeable sodium-ion batteries. *ACS Appl. Mater. Interfaces* **11**, 23520–23526 (2019).
16. Ling, L. *et al.* Quick activation of nanoporous anatase TiO_2 as high-rate and durable anode materials for sodium-ion batteries. *ACS Appl. Mater. Interfaces* **9**, 39432–39440 (2017).
17. Usui, H., Yoshioka, S., Wasada, K., Shimizu, M. & Sakaguchi, H. Nb-doped rutile TiO_2: a potential anode material for Na-ion battery. *ACS Appl. Mater. Interfaces* **7**, 6567–6573 (2015).
18. Bella, F. *et al.* Unveiling the controversial mechanism of reversible Na storage in TiO_2 nanotube arrays: amorphous versus anatase TiO_2. *Nano Res.* **10**, 2891–2903 (2017).
19. Liao, J. Y., Luna, B. D. & Manthiram, A. TiO_2-B nanowire arrays coated with layered MoS_2 nanosheets for lithium and sodium storage. *J. Mater. Chem. A* **4**, 801–806 (2016).
20. Zhang, Y. *et al.* Graphene-rich wrapped petal-like rutile TiO_2 tuned by carbon dots for high-performance sodium storage. *Adv. Mater.* **28**, 9391–9399 (2016).
21. Guo, S., Yi, J., Sun, Y. & Zhou, H. Recent advances in titanium-based electrode materials for stationary sodium-ion batteries. *Energy Environ. Sci.* **9**, 2978–3006 (2016).
22. Yang, Y. *et al.* Carbon dots supported upon N-doped TiO_2 nanorods applied into sodium and lithium ion batteries. *J. Mater. Chem. A* **3**, 5648–5655 (2015).
23. Zhao, Q., Bi, R., Cui, J., Yang, X. & Zhang, L. TiO_{2-x} nanocages anchored in N-doped carbon fiber films as a flexible anode for high-energy sodium-ion batteries. *ACS Appl. Energy Mater.* **1**, 4459–4466 (2018).
24. Cha, H. A., Jeong, H. M. & Kang, J. K. Nitrogen-doped open pore channeled graphene facilitating electrochemical performance of TiO_2 nanoparticles as an anode material for sodium ion batteries. *J. Mater. Chem. A* **2**, 5182–5186 (2014).
25. Wang, J. *et al.* N-doped carbon coated anatase TiO_2 nanoparticles as superior Na-ion battery anodes. *J. Colloid Interface Sci.* **517**, 134–143 (2018).
26. Yeo, Y., Jung, J. W., Park, K. & Kim, I. D. Graphene-wrapped anatase TiO_2 nanofibers as high-rate and long-cycle-life anode material for sodium ion batteries. *Sci. Rep.* **5**, 1–9 (2015).
27. Zhang, Y., Wang, C., Hou, H., Zou, G. & Ji, X. Nitrogen doped/carbon tuning yolk-Like TiO_2 and its remarkable impact on sodium storage performances. *Adv. Energy Mater.* **7**, 1600173 (2017).
28. Xiong, H., Slater, M. D., Balasubramanian, M., Johnson, C. S. & Rajh, T. Amorphous TiO_2 Nanotube anode for rechargeable sodium ion batteries. *J. Phys. Chem. Lett.* **2**, 2560–2565 (2011).
29. Wu, L., Buchholz, D., Bresser, D., Gomes Chagas, L. & Passerini, S. Anatase TiO_2 nanoparticles for high power sodium-ion anodes. *J. Power Sources* **251**, 379–385 (2014).
30. Zhang, Y. *et al.* Boosting sodium storage in TiF_3/carbon core/sheath nanofibers through an efficient mixed-conducting network. *Adv. Energy Mater.* **1901470**, 1–9 (2019).
31. He, H. *et al.* Structure-dependent performance of TiO_2/C as anode material for Na-ion batteries. *Nano Energy* **44**, 217–227 (2018).
32. Wang, H. *et al.* N-doped TiO_2 with a disordered surface layer fabricated via plasma treatment as an anode with clearly enhanced performance for rechargeable sodium ion batteries. *Sustain. Energy Fuels* **3**, 2688–2696 (2019).
33. Wu, Y., Liu, X., Yang, Z., Gu, L. & Yu, Y. Nitrogen-doped ordered mesoporous anatase TiO_2 nanofibers as anode materials for high performance sodium-ion batteries. *Small* **12**, 3522–3529 (2016).
34. Ni, J. *et al.* Self-supported nanotube arrays of sulfur-doped TiO_2 enabling ultrastable and robust sodium storage. *Adv. Mater.* **28**, 2259–2265 (2016).
35. He, H. *et al.* N-doped rutile TiO_2/C with significantly enhanced Na storage capacity for Na-ion batteries. *Electrochim. Acta* **236**, 43–52 (2017).
36. Yan, D. *et al.* Enhanced electrochemical performances of anatase TiO_2 nanotubes by synergetic doping of Ni and N for sodium-ion batteries. *Electrochim. Acta* **254**, 130–139 (2017).

37. Liu, S., Cai, Z., Zhou, J., Pan, A. & Liang, S. Nitrogen-doped TiO_2 nanospheres for advanced sodium-ion battery and sodium-ion capacitor applications. *J. Mater. Chem. A* **4**, 18278–18283 (2016).
38. Wang, B. *et al.* Boron-doped anatase TiO_2 as a high-performance anode material for sodium-ion batteries. *ACS Appl. Mater. Interfaces* **8**, 16009–16015 (2016).
39. Cao, M. *et al.* Phosphorus-doped TiO_2-B nanowire arrays boosting robust pseudocapacitive properties for lithium storage. *J. Power Sources* **396**, 327–334 (2018).
40. Wang, Q. *et al.* Synergistic effect of N-doping and rich oxygen vacancies induced by nitrogen plasma endows TiO_2 superior sodium storage performance. *Electrochim. Acta* **309**, 242–252 (2019).
41. Yan, Y. *et al.* Understanding the fast lithium storage performance of hydrogenated TiO_2 nanoparticles. *J. Mater. Chem. A* **1**, 14507–14513 (2013).
42. Wang, H. *et al.* Disordered surface formation of WS_2 Via hydrogen plasma with enhanced anode performances for lithium and sodium ion batteries. *Sustain. Energy Fuels* **3**, 865–874 (2019).
43. Yan, Y. *et al.* Slightly hydrogenated TiO_2 with enhanced photocatalytic performance. *J. Mater. Chem. A* **2**, 12708–12716 (2014).
44. Bineesh, K. V., Kim, D.-K. & Park, D.-W. Synthesis and characterization of zirconium-doped mesoporous nano-crystalline TiO_2. *Nanoscale* **2**, 1222–1228 (2010).
45. Zhang, Z. L. *et al.* Enhancement of perovskite solar cells efficiency using N-doped TiO_2 nanorod arrays as electron transfer layer. *Nanoscale Res. Lett.* **12**, 43 (2017).
46. Hu, Y. *et al.* Synthesis and photoelectrochemical response of CdS quantum dot-sensitized TiO_2 nanorod array photoelectrodes. *Nanoscale Res. Lett.* **8**, 1–5 (2013).
47. Yao, X., Wang, X., Su, L., Yan, H. & Yao, M. Band structure and photocatalytic properties of N/Zr co-doped anatase TiO_2 from first-principles study. *J. Mol. Catal. A Chem.* **351**, 11–16 (2011).
48. Huang, D. G. *et al.* Synthesis of samarium- and nitrogen-co-doped TiO_2 by modified hydrothermal method and its photocatalytic performance for the degradation of 4-chlorophenol. *J. Phys. Chem. Solids* **70**, 853–859 (2009).
49. Singhal, R. K., Kumar, S., Kumari, P., Xing, Y. T. & Saitovitch, E. Evidence of defect-induced ferromagnetism and its 'switch' action in pristine bulk TiO_2. *Appl. Phys. Lett.* **98**, 1–4 (2011).
50. Battiston, G. A. *et al.* PECVD of amorphous TiO_2 thin films: effect of growth temperature and plasma gas composition. *Thin Solid Films* **371**, 126–131 (2000).
51. Chen, X. & Burda, C. Photoelectron spectroscopic investigation of nitrogen-doped titania nanoparticles. *J. Phys. Chem. B* **108**, 15446–15449 (2004).
52. Sakthivel, S., Janczarek, M. & Kisch, H. Visible light activity and photoelectrochemical properties of nitrogen-doped TiO_2. *J. Phys. Chem. B* **108**, 19384–19387 (2004).
53. Cong, Y., Zhang, J., Chen, F. & Anpo, M. Synthesis and characterization of nitrogen-doped TiO_2 nanophotocatalyst with high visible light activity. *J. Phys. Chem. C* **111**, 6976–6982 (2007).
54. Oh, S. M. *et al.* High electrochemical performances of microsphere C-TiO_2 anode for sodium-ion battery. *ACS Appl. Mater. Interfaces* **6**, 11295–11301 (2014).
55. Kim, K. T. *et al.* Anatase titania nanorods as an intercalation anode material for rechargeable sodium batteries. *Nano Lett.* **14**, 416–422 (2014).
56. Lin, J. *et al.* In situ nitrogen doping of TiO_2 by plasma enhanced atomic layer deposition for enhanced sodium storage performance. *Dalton Trans.* **46**, 13101–13107 (2017).
57. Wu, Y., Liu, X., Yang, Z., Gu, L. & Yu, Y. Nitrogen-doped ordered mesoporous anatase TiO_2 nanofibers as anode materials for high performance sodium-ion batteries. *Small* https://doi.org/10.1002/smll.201670126 (2016).
58. Wu, C. *et al.* Insight into the origin of capacity fluctuation of $Na_2Ti_6O_{13}$ anode in sodium ion batteries. *ACS Appl. Mater. Interfaces* **9**, 43596–43602 (2017).
59. Soto, F. A. *et al.* Tuning the solid electrolyte interphase for selective Li- and Na-ion storage in hard carbon. *Adv. Mater.* **29**, 1606860 (2017).
60. Cui, X. *et al.* Improving Mn tolerance of lithium-ion batteries by using lithium bis(oxalato)borate-based electrolyte. *Electrochim. Acta* **253**, 291–301 (2017).

Acknowledgements

Author contributions
D.W., G.C. and P.S. initiated and coordinated the study. H.W. and J.X. prepared the samples, H.W. and X.C. performed the electrochemical measurements, and T.K. conducted the TEM investigation. H.W., D.W. and G.C. co-wrote the manuscript. All authors discussed the results and commented on the manuscript.

Competing interests
The authors declare no competing interests.

Additional information
Correspondence and requests for materials should be addressed to G.C. or D.W.

Reprints and permissions information is available at www.nature.com/reprints.

Publisher's note Springer Nature remains neutral with regard to jurisdictional claims in published maps and institutional affiliations.